#### **Research Article**

Sahw S. Almutairi, Ahmed O. Mosleh, Samah Samir Mohamed, Tamer Samir Mahmoud, and Essam B. Moustafa\*

# Max-phase Ti<sub>3</sub>SiC<sub>2</sub> and diverse nanoparticle reinforcements for enhancement of the mechanical, dynamic, and microstructural properties of AA5083 aluminum alloy *via* FSP

https://doi.org/10.1515/ntrev-2024-0130 received June 5, 2024; accepted November 14, 2024

Abstract: This study investigated the effects of max-phase Ti<sub>3</sub>SiC<sub>2</sub> and other nanoparticle reinforcements (graphene, CNTs, and SiN) on the mechanical and dynamic properties of friction stir processed (FSPed) AA5083 aluminum composites. Microstructural analysis revealed the impact of these reinforcements on grain size. Dynamic properties were assessed using a free vibration impact test, while mechanical properties were measured through a compression test. Most composites showed enhancements in damping ratio and natural frequency compared to the base alloy, with the Ti<sub>3</sub>SiC<sub>2</sub> leading to a substantial increase in natural frequency. The AA5083/max phase Ti<sub>3</sub>SiC<sub>2</sub> composite demonstrated the most significant improvements across nearly all properties, notably enhancing stiffness (+7.35% in E), strength (+25.36% in yield strength), and vibration resistance (+5.83% in  $f_n$ ), while significantly reducing damping (-62.76% in  $\zeta$ ). In contrast, the friction stirred AA5083 offered moderate enhancements in strength (+17.86% in yield strength) and a slight increase in natural frequency (+2.00%) but did not significantly improve stiffness and actually increased damping. The base alloy AA5083 served as the baseline for comparison, exhibiting the lowest performance in all categories. The findings highlight the potential of FSP and reinforcement, especially Ti<sub>3</sub>SiC<sub>2</sub>, for tailoring the properties of AA5083 for enhanced performance in various applications. These findings emphasize the significance of customizing

**Keywords:** max-phase Ti<sub>3</sub>SiC<sub>2</sub>, dynamic properties, mechanical properties, microstructure, CNTs, graphene, SiN, nanocomposites

# 1 Introduction

Aluminum alloys are considered as one of the most important metals used nowadays with regard to their relative strength and low density compared to other metals. In this regard, AA5083 aluminum is compared to other marine alloys such as mild steel and stainless steel, and chipping of this material can significantly damage the tool [1,2]. AA5083 is a popular aluminum alloy because it is inexpensive and corrosion-resistant to seawater. It is most commonly used in the maritime sector worldwide. Due to rapid corrosion, high-quality materials are expensive but can extend the product's life; hence, mild steel trawler rudders rarely last longer than 3 years [3]. The fittings for the pin and sliding rudders show rapid corrosion of mild steel within 2 years [4].

In contrast, rudders constructed of AA5083 alloy that is welded and corrosion resistant have functioned for 6 years with minimal maintenance [5,6]. However, the AA5083 alloys need to be upgraded to handle high loads and operating circumstances. Friction stir processing is a technique used to enhance the strength of aluminum alloy [7,8]. This is achieved by incorporating minuscule ceramic nanoparticles, such as silicon carbide (SiC) or aluminum oxide (Al $_2$ O $_3$ ), into the mixture [9]. The quantity of these particles introduced is crucial, as it directly impacts the strength of the resulting material [10,11]. Many researchers have developed single or hybrid composites; thus, they reinforce the AA5083 with ceramic particles and nanoparticles to enhance its mechanical properties [12–15]. Several reinforcing

the reinforcement material to attain the intended mechanical characteristics in AA5083 composites.

<sup>\*</sup> Corresponding author: Essam B. Moustafa, Mechanical Engineering Department, Faculty of Engineering, King Abdulaziz University, PO Box 80204, Jeddah, Saudi Arabia, e-mail: abmostafa@kau.edu.sa Sahw S. Almutairi, Ahmed O. Mosleh, Samah Samir Mohamed, Tamer Samir Mahmoud: Mechanical Engineering Department, Faculty of Engineering at Shoubra, Benha University, Cairo, 11629, Egypt

2 — Sahw S. Almutairi *et al.* DE GRUYTER

particles are used to improve various properties. Tungsten carbide (WC), tantalum carbide, niobium carbide, vanadium, SiC, Al<sub>2</sub>O<sub>3</sub>, boron carbide, titanium carbide, and zirconium carbide have excellent compatibility with aluminum alloys [16-21]. The friction stir technique fabricates AA5083 surface composites enhanced with carbon nanotubes (CNTs) and cerium oxide microparticles. The hybrid composite with a 75–25% volume ratio of CNTs and cerium oxide produced the highest tensile strength and hardness values [22]. Another investigation demonstrates the powder metallurgy approach as a new method for creating a high-strength aluminum composite reinforced with nano-sized titanium diboride (TiB<sub>2</sub>) particles [23]. Using powder metallurgy, a homogeneous dispersion of multi-walled carbon nanotubes (MWCNTs) throughout the aluminum alloy AA5083 matrix is crucial for enhancing the mechanical properties of the composite [24]. Friction stir process (FSP) enhanced the surface hardness and wear resistance of aluminum alloy 5083 using ceramic reinforcements such as SiC, Al<sub>2</sub>O<sub>3</sub>, and a combination. Among these, the 50% SiC and 50% Al<sub>2</sub>O<sub>3</sub> hybrid composite exhibited the most favorable outcomes [25]. FSP incorporating WC-Al<sub>2</sub>O<sub>3</sub> ceramic composite into AA5083 significantly improved hardness and wear resistance. The process refines the grain structure and distributes the reinforcement particles more uniformly, leading to a maximum hardness of 55% higher than the base metal [26].

Several studies have explored enhancing aluminum alloys' damping capacity [27,28]. One study incorporating interconnected reinforcements, such as galvanized iron wire preforms, significantly improves vibration absorption [29]. The iron oxide particles, specifically at a size of 500 nm and a concentration of 4 wt%, offer the most promising results regarding dynamic behavior modification within the aluminum matrix [30]. The influence of titanium (Ti) inclusion on damping characteristics on aluminum composites reinforced with in situ formed TiB<sub>2</sub> particles [30]. This research examines how different reinforcing materials influence the properties of aluminum matrix composites. These materials include master alloys, metalceramic aggregates, nanofibrous composites, and those produced through squeeze casting. Their findings suggest that these reinforcements can improve the damping response, the composites' mechanical properties, and wear characteristics [31]. This study aims to create surface metal matrix composites (MMCs) with superior performance on AA5083 alloy by using FSP. The study aims to investigate the impact of different types, concentrations, and distributions of single nanoparticles (graphene, silicon nitride [SiN], and CNT nanoparticles) and their hybrid combinations on the composites' mechanical properties and dynamic behavior. The novelty of this work lies in the systematic investigation of the combined effects of the FSP and various reinforcements, including single and hybrid particles, on both the dynamic

modulus and ultimate compression strength of AA5083 aluminum alloy. This comprehensive approach provides valuable insights into the potential for tailoring the mechanical properties of this alloy for specific applications through microstructural modification and reinforcement strategies. The study also highlights the complex interplay between different types of reinforcements and their impact on the resulting properties, emphasizing the need for careful selection and optimization of reinforcement combinations to achieve desired performance outcomes.

## 2 Materials and methods

## 2.1 Materials and fabrication process

A novel MMCs can be fabricated using the FSP by reinforcing wrought aluminum alloy AA5083 sheets with a combination of max-phase Ti<sub>3</sub>SiC<sub>2</sub> particles, graphene, CNTs, and SiN nanoparticles. AA5083 aluminum alloy sheets with a thickness of  $150 \times 150 \times 10 \text{ mm}^3$  were utilized as the base matrix material. The reinforcement nanoparticles, such as the max-phase Ti<sub>3</sub>SiC<sub>2</sub> particles with an average size of 80 nm, were chosen due to their excellent mechanical properties, including high hardness, thermal stability, and good wear resistance [24]. Graphene with a lateral size of 2 µm and a thickness of 1.5 nm was employed for its potential to enhance strength and electrical conductivity [32,33]. The CNT particles with a diameter of 15 nm and a length of 2.15 µm were selected for their exceptional strength, high aspect ratio, and potential for improving the composite's load-bearing capacity [34,35]. Finally, the SiN, with an average size of 40 nm, was incorporated to enhance the composite's wear resistance and thermal stability due to its excellent hardness and chemical inertness [36].

The process commences with substrate preparation, where the AA5083 sheets are cut to desired dimensions, cleaned with a solvent, and drilled with a regular pattern of holes having a specified diameter (*e.g.*, 3 mm) and depth (*e.g.*, 3 mm) to accommodate the reinforcement mixture. The reinforcement mixture is prepared by precisely weighing and measuring the required quantities of each component (Ti<sub>3</sub>SiC<sub>2</sub> particles, graphene, CNTs, and SiN nanoparticles) according to the desired weight fraction in the final composite. Subsequently, a micropipette or similar dispensing tool is employed to meticulously transfer the measured amount of the reinforcement mixture into each pre-drilled hole, ensuring complete filling. In parallel, the FSP tool is fabricated from tool steel based on specific design criteria, typically incorporating a triangular pin profile and a designated

tilt angle (e.g., 3°). The AA5083 sheet with filled holes is then secured onto the milling machine bed, and the fabricated FSP tool is mounted onto the spindle. With the processing parameters established through successful trial runs (e.g., 800 rpm tool rotation speed, 30 mm/min tool traverse speed, and 3° tilt angle), the FSP process commences by plunging the tool into the designated starting point on the sheet (Figure 1). The tool traverses along a predefined path at a constant speed while rotating and stirring the material at the set parameters to achieve complete coverage of the desired area. Following FSP, the processed area is allowed to cool. The processed sheets can undergo further machining or grinding to attain the final dimensional requirements.

#### 2.2 Characterization

Metallographic preparation involving mechanical grinding with SiC paper, polishing, and etching using standard reagents was employed to characterize the microstructure of the composite materials, as shown in detail in previous study [37]. The prepared samples were subsequently examined using JEOL scanning electron microscopy (SEM) and Olympus BX51 optical microscopy for a comprehensive microstructural analysis. The grain size was measured using the linear intercept method. The compression test is used to assess the mechanical properties. The universal

testing machine (UTM) (SANS) utilized in this study is equipped with a load cell for application load measurement and a displacement transducer for sample deformation measurement. A computer can conveniently operate the UTM by applying different loading conditions.

## 2.3 Dynamic test setup

The dynamic properties of the composite materials were evaluated by performing a free vibration test following the ASTM E756-05 guidelines. This test method offers a non-destructive evaluation of a material's inherent stiffness and damping characteristics by measuring its natural frequencies [28,38-41]. The experiment included samples with a regular rectangular crosssection beam, which had dimensions of 100 mm in length, 8 mm in breadth, and 6 mm in thickness. The test specimen was constructed as a cantilever beam, with one side firmly fixed and the other free to move. The B&K model 4507-B accelerometer was attached to the free end of the cantilever beam to measure its response over time. The composite beam was vibrated using a B&K model 8206 impulse hammer. The following vibration response was monitored and studied using an impulse data analyzer (B&K module 3160-A-4/2). Figure 2 illustrates the complete experimental setup; thus the acquired data were analyzed using ME'Scope, a software designed for modal analysis. This software facilitates calculating the frequency response function (FRF), damping ratio, and fundamental frequencies. To ensure

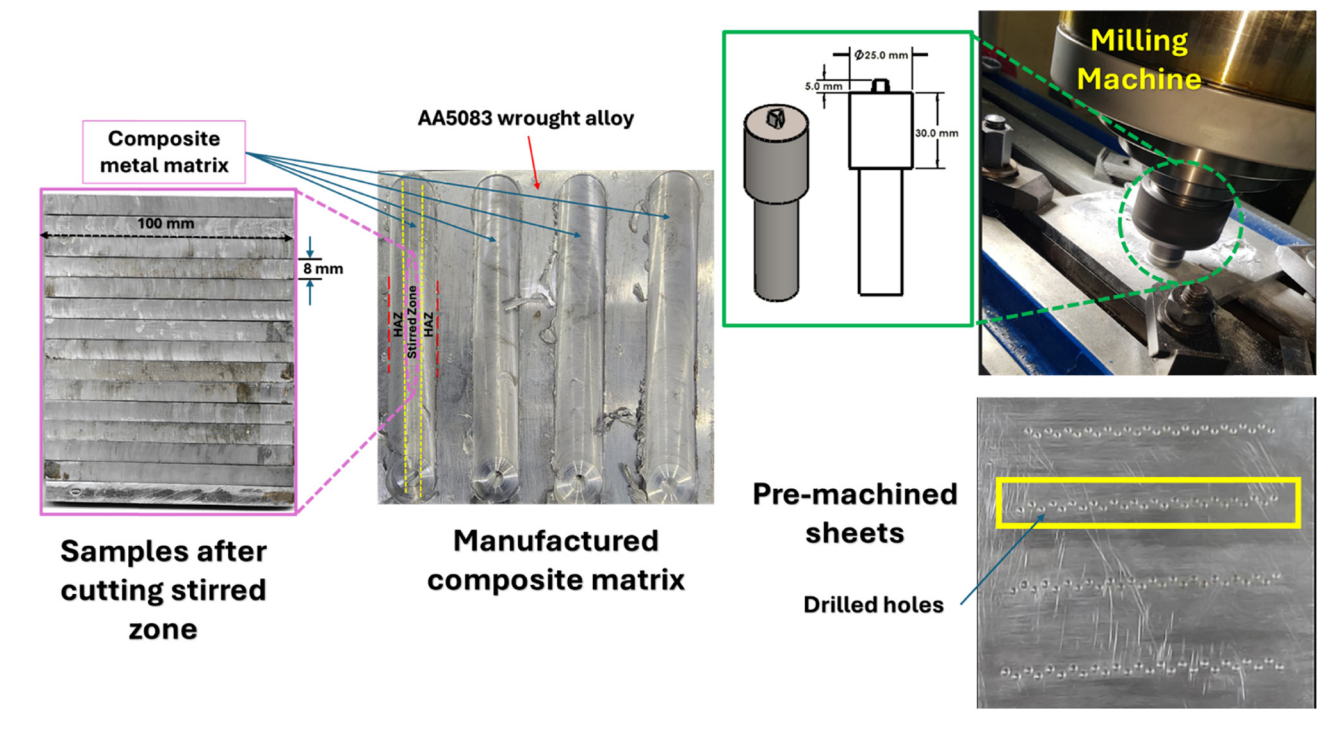


Figure 1: Fabrication process of the investigated MMNCs.

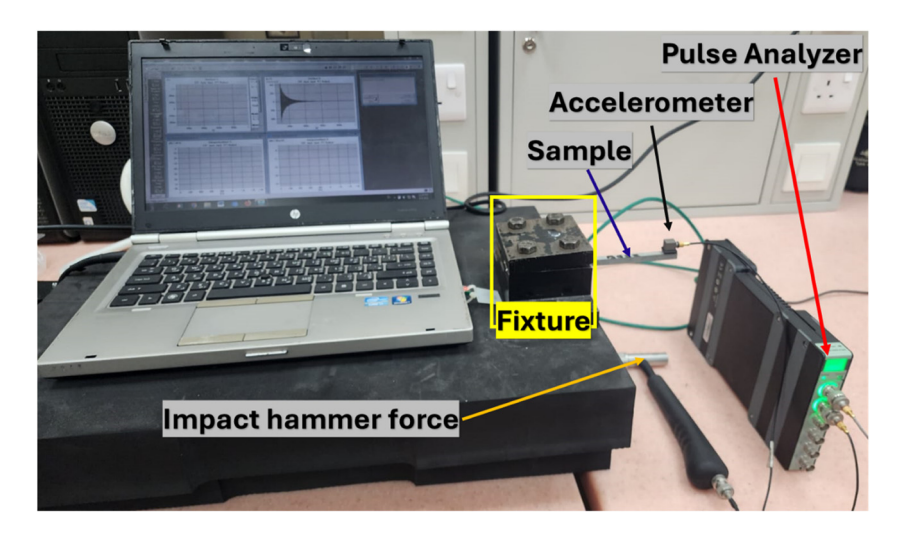


Figure 2: Free vibration impact test setup.

the accuracy of the results, the free vibration test was carried out five distinct times. The mean outcomes of these repeated trials were subsequently employed to establish correlations between the material properties and the measured variables.

## 3 Results and discussion

#### 3.1 Microstructure observation

The microstructure of the FSP samples is categorized into three clearly defined regions: the heat-affected zone (HAZ), the thermomechanically affected zone (TMHAZ), and the stirred zone (SZ), as shown in Figure 3. The heat generated by the FSP tool causes a substantial increase in temperature in the HAZ, but the HAZ is not subjected to the stirring action. This area may experience either grain coarsening or

softening, depending on the processing settings and characteristics of the base metal [42,43]. The TMHAZ undergoes both frictional heating and stirring, leading to a partially recrystallized microstructure that may have finer grains than HAZ. Ultimately, the SZ experiences the most notable alteration in shape and temperature due to intense plastic deformation and frictional heating. This results in a substantial reduction in grain size and the possibility of a transformation in grain structure. The SZ is the central area where the FSP tool directly interacts with the material, resulting in substantial changes to its microstructure.

The CNTs, graphene, and SiN particles exhibit distinct differences in size and distribution, influencing their reinforcing effects. CNTs have a fine, elongated morphology but some agglomeration potentially limiting their full potential. Graphene platelets show a more even distribution and better interfacial bonding, but restacking can compromise their effectiveness. SiN particles are smaller and

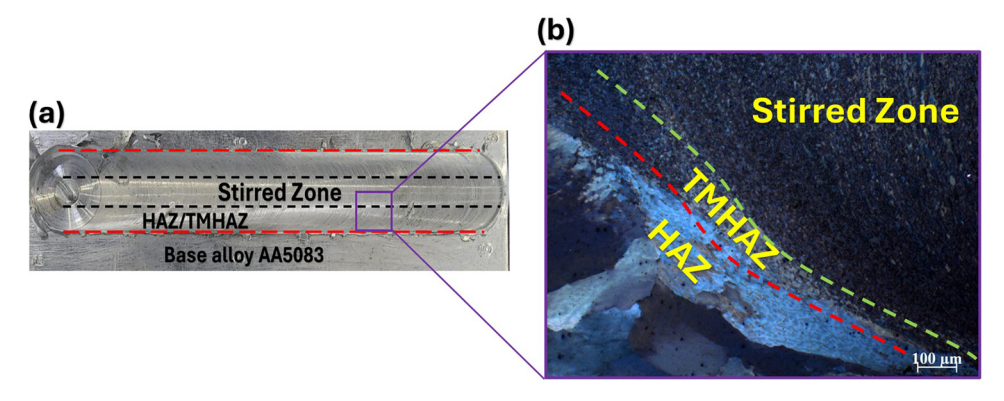


**Figure 3:** Microstructural zones in FSP. (a) Illustration of the microstructure zones in the FSP sample. (b) Typical image of the microstructure zones with the main three zones: the HAZ, the TMHAZ, and the SZ are the core region directly affected by the FSP tool.

more uniformly dispersed, enhancing strength and wear resistance. In hybrid composites, combining different reinforcements can lead to synergistic effects or trade-offs. For instance, Ti<sub>3</sub>SiC<sub>2</sub>+SiN resulted in the most homogenous distribution, suggesting superior properties, while Ti<sub>3</sub>SiC<sub>2</sub>+CNTs showed a less uniform dispersion, potentially limiting synergistic effects. These differences in mechanical properties between single and hybrid composites are attributed to particle size, morphology, and distribution variations, influencing the network of pinning sites and overall grain structure.

Figure 4 shows the optical microstructure images of the investigated sample inside the SZ; thus, microscopic analysis reveals a dramatic transformation in the microstructure of AA5083 upon FSP. The original rolled sheet exhibits elongated grains aligned with the rolling direction (Figure 4a). The recrystallization process within the processed zone is facilitated using frictional heat generated by a rotating tool and stirring action. The results show a dramatic grain size refinement in the SZ of all the samples processed by FSP compared to the base AA5083 metal (Figure 4b). The base metal has a coarse grain size of 300  $\mu m$  with an aspect ratio of 2.1,

indicating elongated grains. FSP itself (FSPed AA5083) resulted in a significant grain refinement down to 6.28  $\mu m$ , a reduction of over 97% compared to the base metal. This refinement is attributed to dynamic recrystallization, a process where the severe plastic deformation caused by the FSP tool creates high dislocation densities within the material. These dislocations act as nucleation sites for new, finer grains to form.

Interestingly, the addition of max-phase  $Ti_3SiC_2$  particles, either as a single reinforcement (AA5083/ $Ti_3SiC_2$ ) or in combination with other reinforcements in the hybrid composites (AA5083/ $Ti_3SiC_2$ +G, AA5083/ $Ti_3SiC_2$ +SiN, AA5083/ $Ti_3SiC_2$ +CNTs), resulted in a slightly smaller grain size compared to FSPed AA5083 alone. This could be due to several factors. The presence of the particles might hinder the movement of dislocations, reducing their effectiveness as nucleation sites. Additionally, the reinforcement particles might introduce some pinning force that prevents the complete refinement of the grains. However, the grain size in all the reinforced composites (4.3–5.7  $\mu$ m) is still significantly smaller than the base metal, achieving a refinement of

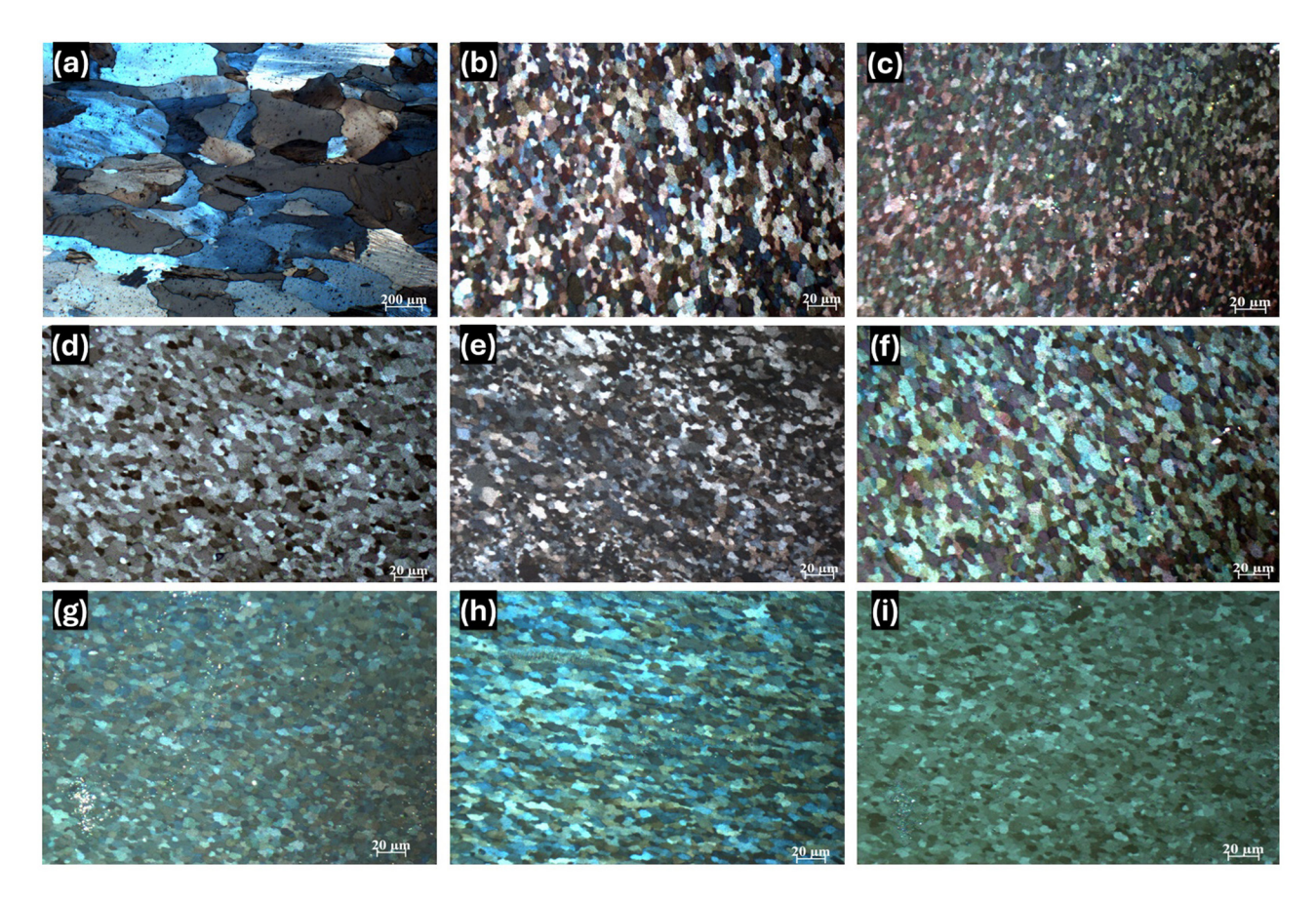


Figure 4: Optical microstructural images of the samples (a) AA5083 base alloy; the images inside the SZ, (b) FSPed AA5083, (c) AA5083/Ti<sub>3</sub>SiC<sub>2</sub>, (d) AA5083/G, (e) AA5083/CNTs, (f) AA5083/SiN, (g) AA5083/Ti<sub>3</sub>SiC<sub>2</sub>+G, (h) AA5083/Ti<sub>3</sub>SiC<sub>2</sub>+CNTs, and (i) AA5083/Ti<sub>3</sub>SiC<sub>2</sub>+SiN.

over 94%. Among the reinforced composites, the secondary reinforcements (graphene, SiN, and CNTs) seem to have minimal influence on the final grain size. They all resulted in a grain size of around 5 µm, with the hybrid composite containing CNTs showing a slightly larger size (Figure 5). It is important to note that the aspect ratio of all FSP processed samples is close to 1, indicating more equiaxed grains than the base metal's elongated grains. This change in grain morphology can significantly improve the material's mechanical properties. The presence of multiple reinforcement types with varying sizes, shapes, and distributions could create a more intricate network of pinning sites within the microstructure, potentially leading to a stronger collective force on grain boundaries [44]. Additionally, hybrid composites might offer a more uniform dispersion of pinning sites throughout the matrix, ensuring a consistent pinning effect, and resulting in a more homogenous and finer grain structure.

#### 3.2 SEM observation

Figure 6 visually represents the microstructural characteristics and reinforcement particle distribution within various AA5083 composites. In the single composites (a)–(c), the CNTs in AA5083/CNTs (a) exhibit a fine, elongated

morphology with some agglomeration, while the graphene platelets in AA5083/G (b) display a more even distribution and layered structure, suggesting better interfacial bonding. The SiN particles in AA5083/SiN (c) are smaller and more uniformly dispersed than CNTs and graphene, potentially leading to enhanced strength and wear resistance. The hybrid composites (d)-(f) reveal the combined effects of different reinforcements. AA5083/Ti<sub>3</sub>SiC<sub>2</sub>+CNTs (d) show a mix of well-distributed Ti<sub>3</sub>SiC<sub>2</sub> particles and less uniformly dispersed CNTs. AA5083/Ti<sub>3</sub>SiC<sub>2</sub>+G (e) exhibits a more uniform distribution of both Ti<sub>3</sub>SiC<sub>2</sub> and graphene, potentially resulting in improved synergistic effects. Notably, AA5083/Ti<sub>3</sub>SiC<sub>2</sub>+SiN (f) demonstrates the most homogeneous distribution of all reinforcements, with fine SiN particles evenly dispersed and Ti<sub>3</sub>SiC<sub>2</sub> particles well-integrated, suggesting superior mechanical properties and microstructural stability due to improved load transfer and reduced stress concentration. These observations highlight the significant influence of reinforcement type and combination on the microstructure and potential properties of AA5083 composites, warranting further investigation into the structure-property relationships through mechanical testing and detailed characterization.

The investigation demonstrates the effective integration of reinforcing particles into the manufactured metal matrix. The presence of max-phase Ti<sub>3</sub>SiC<sub>2</sub> particles throughout the matrix is confirmed by energy dispersive X-ray spectroscopy

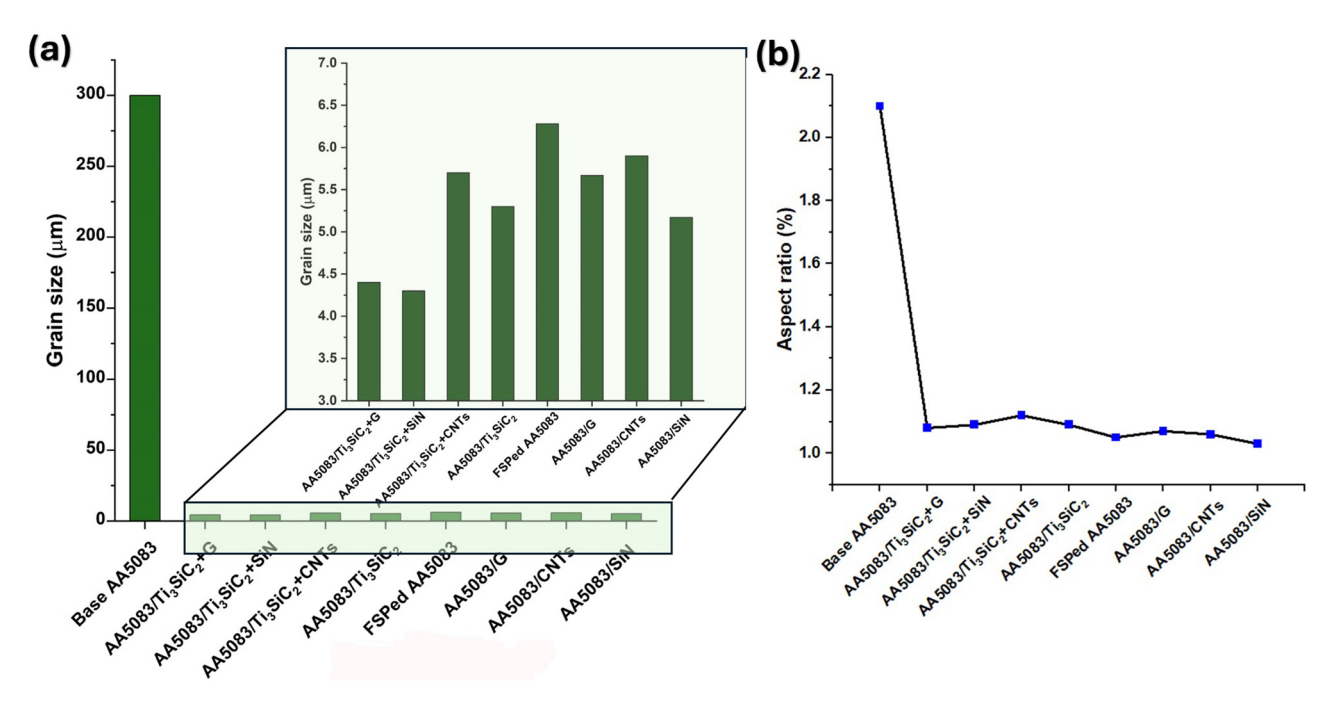


Figure 5: Effect of FSP on grain size and aspect ratio in AA5083 composites with various reinforcements: (a) grain size histogram and (b) aspect ratio.

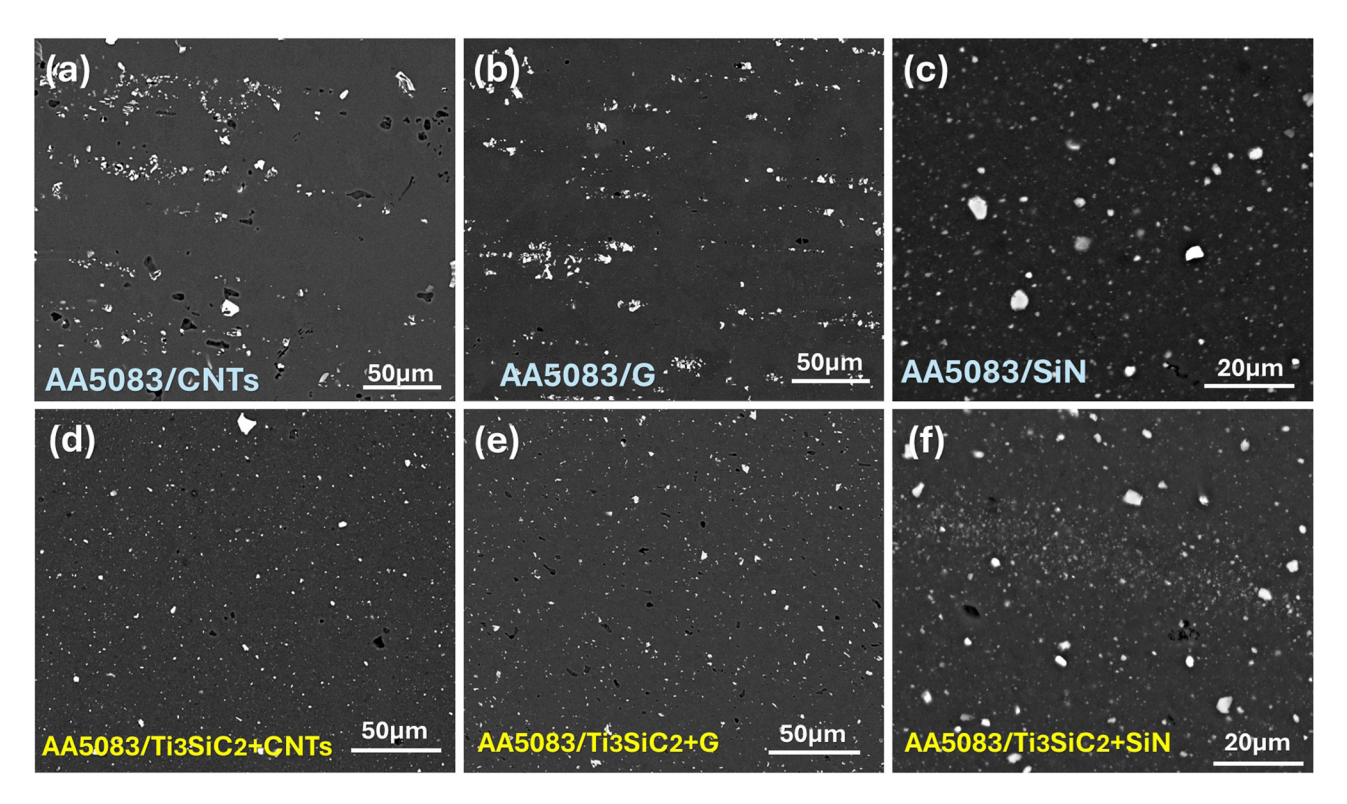


Figure 6: SEM images of the single composites: (a) AA5083/CNTs, (b) AA5083/G, (c) AA5083/SiN and hybrid composite with max phase particles, (d) AA5083/Ti<sub>3</sub>SiC<sub>2</sub>+CNTs, (e) AA5083/Ti<sub>3</sub>SiC<sub>2</sub>+G, and (f) AA5083/Ti<sub>3</sub>SiC<sub>2</sub>+SiN.

(EDX) research, confirming their effective distribution. The probable cause of this phenomenon is the agitating effect of the FSP process, which aids in the dispersion of particles and inhibits their aggregation. Furthermore, Figure 7 provides visual evidence of the existence of SiN particles within the matrix, reinforcing the successful incorporation of these reinforcements. Nevertheless, the EDX examination exclusively identifies the existence of the carbon element in graphene and CNTs. This does not always imply a deficiency in these reinforcements. Because of their smaller size and potentially lower concentration relative to other reinforcements, individually identifying them in the EDX study may be more difficult. The EDX spectrum in Figure 7 clearly shows a Si peak, but the Ti peak is less prominent, potentially due to the lower weight percentage of Ti in the Ti<sub>3</sub>SiC<sub>2</sub> reinforcement compared to Si, leading to a weaker Ti signal. Additionally, peak overlap with other elements like Al might obscure the Ti peak. While EDX alone may not conclusively prove the presence of Ti, the SEM images clearly show the distinct morphology and distribution of Ti<sub>3</sub>SiC<sub>2</sub> particles. These observations and the Si signal strongly support the successful incorporation of Ti<sub>3</sub>SiC<sub>2</sub>. To further confirm the presence and distribution of Ti, the energy-dispersive X-ray mapping (EDX mapping) is employed, with the spatial distribution of Ti within the composite as shown in Figure 8.

# 3.3 Mechanical properties

Figure 9 shows the investigated samples' ultimate and yield compressive strength at various deformations. This diagram illustrates a comparison of the mechanical characteristics of the produced composites. Subplots (a) and (c) depict the ultimate compressive strength (UCS) of the single and hybrid composites, respectively. The measurements were taken at both 30 and 60% distortion. Subplots (b) and (d) specifically examine the yield stress of the single and hybrid composites, respectively, at a specific strain of  $\sigma_{0.2\%}$ . The base AA5083 alloy, characterized by a yield strength of 280 MPa and ultimate strengths of 900 MPa (at 60% deformation) and 478 MPa (at 30% deformation), is a benchmark for comparison. The FSP significantly enhances the alloy's performance, leading to a notable 17.9% increase in yield strength (330 MPa), a 12.8% increase in ultimate strength at 60% deformation (1,015 MPa) and a 12.6% increase in ultimate strength at 30% deformation (538 MPa). This improvement is attributed to grain refinement and microstructural homogenization induced by the FSP process, which promotes increased dislocation density and enhanced resistance to plastic deformation. Incorporating reinforcing agents, both single reinforcement and hybrid combinations further elevate the mechanical properties. Notably, the AA5083/Ti<sub>3</sub>SiC<sub>2</sub> composite exhibits a

8 — Sahw S. Almutairi et al. DE GRUYTER

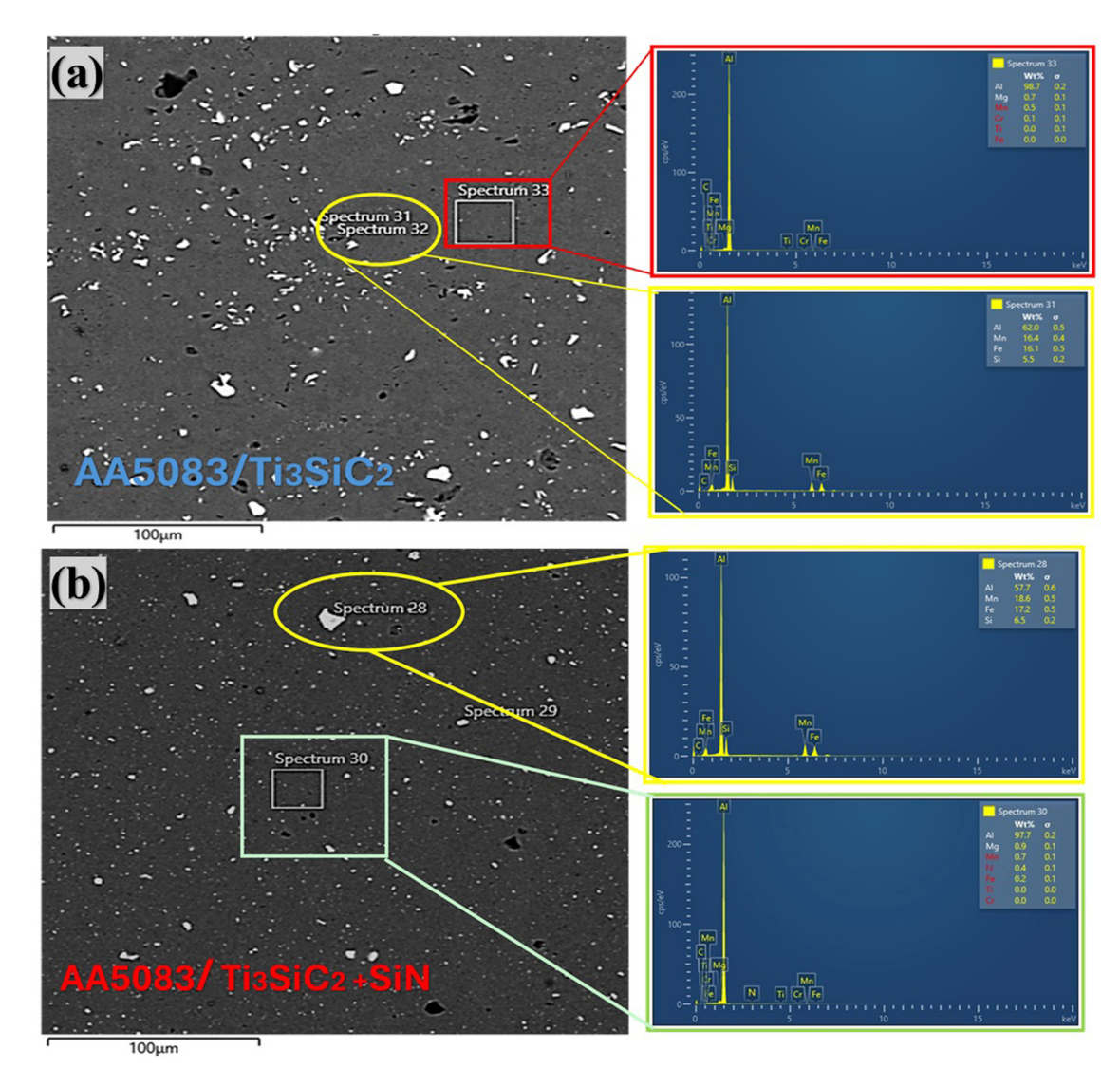


Figure 7: SEM and EDX analysis of (a) single composite AA5083/Ti<sub>3</sub>SiC<sub>2</sub> and (b) hybrid AA5083/Ti<sub>3</sub>SiC<sub>2</sub>+SiN.

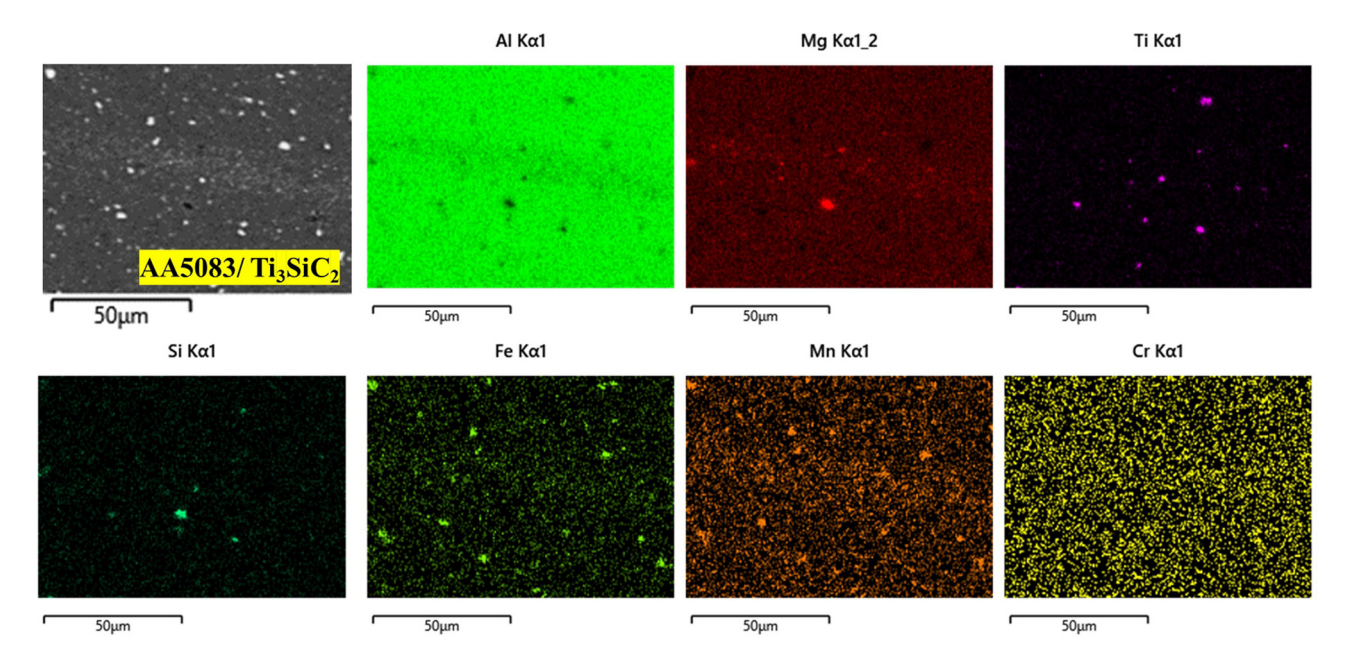
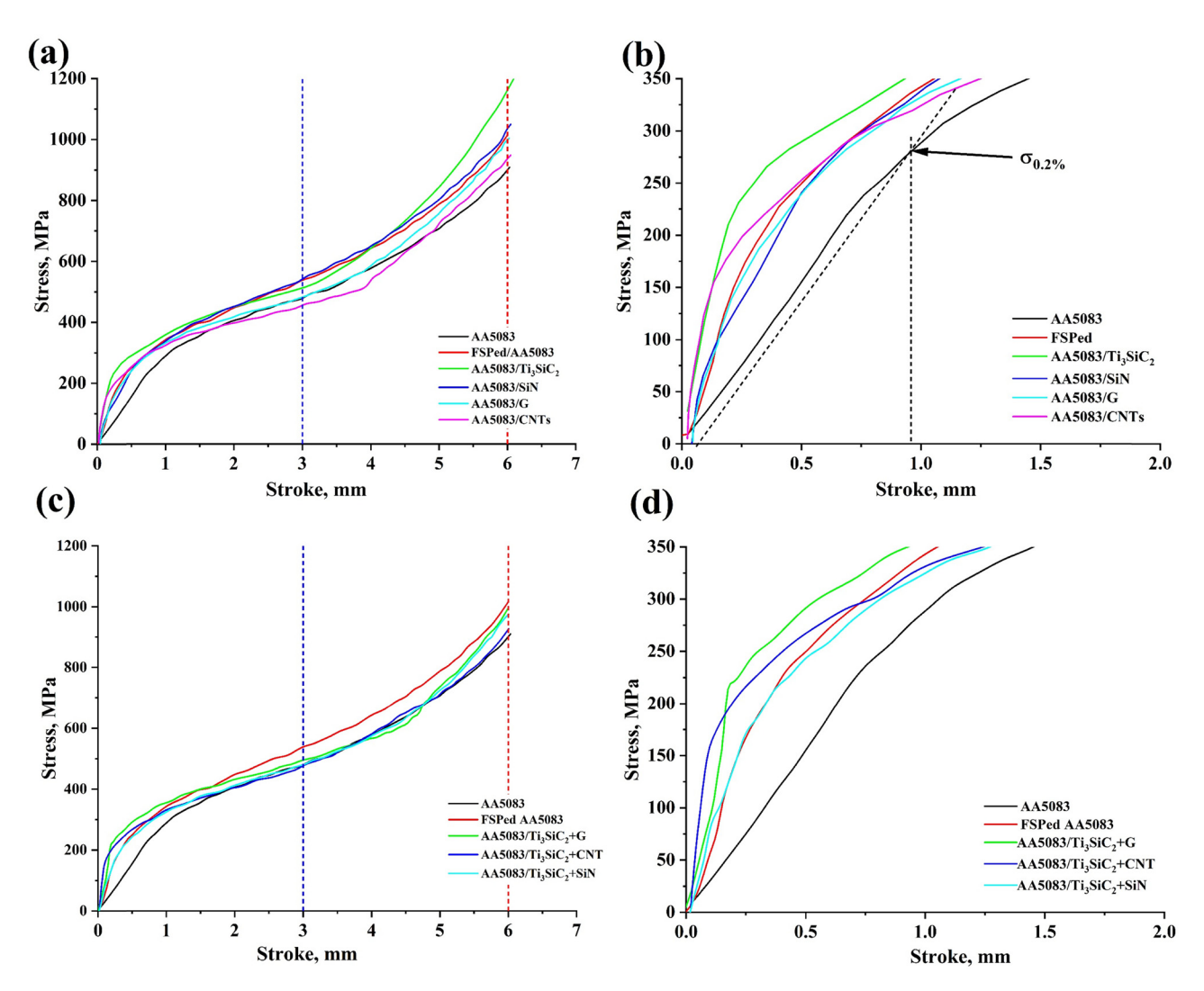


Figure 8: SEM images of the elemental mapping taken inside the SZ for the single composite AA5083/Ti<sub>3</sub>SiC<sub>2</sub>.



**Figure 9:** Ultimate and yield strength of the investigated samples at different deformation percentages: (a) UCS of the single composite at 30 and 60% deformation, (b) yield stress of the single composite at  $\sigma_{0.2\%}$ , (c) UCS of the hybrid composites at 30 and 60% deformation, and (d) yield stress of the hybrid composites at  $\sigma_{0.2\%}$ .

substantial 25.4% increase in yield strength (351 MPa) and a remarkable 29.1% increase in ultimate strength at 60% deformation (1,162 MPa) compared to the base alloy (Figure 10). This exceptional performance can be attributed to the strong interfacial bonding between the Ti<sub>3</sub>SiC<sub>2</sub> particles and the aluminum matrix and the particles' ability to impede dislocation motion, thereby promoting strain hardening. The hybrid composite AA5083/Ti<sub>3</sub>SiC<sub>2</sub>+G demonstrates a comparable yield strength to the AA5083/ Ti<sub>3</sub>SiC<sub>2</sub> composite (350 MPa), highlighting the potential of hybrid reinforcement strategies to tailor mechanical properties. However, it is crucial to note that the ultimate compression strengths at 30% deformation for most single and hybrid composites are comparable or marginally lower than the FSPed AA5083. This observation suggests a potential tradeoff between strength and ductility, wherein the reinforcing particles while enhancing strength, might impede plastic deformation at higher strain levels. Furthermore, while exhibiting promising yield strengths, the hybrid composites generally display lower ultimate strengths than their single-reinforcement counterparts, indicating that combining multiple reinforcements may not always lead to synergistic effects.

Observing lower ultimate strengths in hybrid composites than in single-reinforcement composites highlights potential trade-offs in hybrid reinforcement strategies. While hybrid composites offer the possibility of synergistic property enhancements, combining different reinforcements can lead to lower ultimate strengths due to several factors. These include interfacial interactions between different reinforcement types, where incompatibility in thermal expansion or chemical bonding can cause stress concentrations and premature failure. Additionally, achieving uniform dispersion of

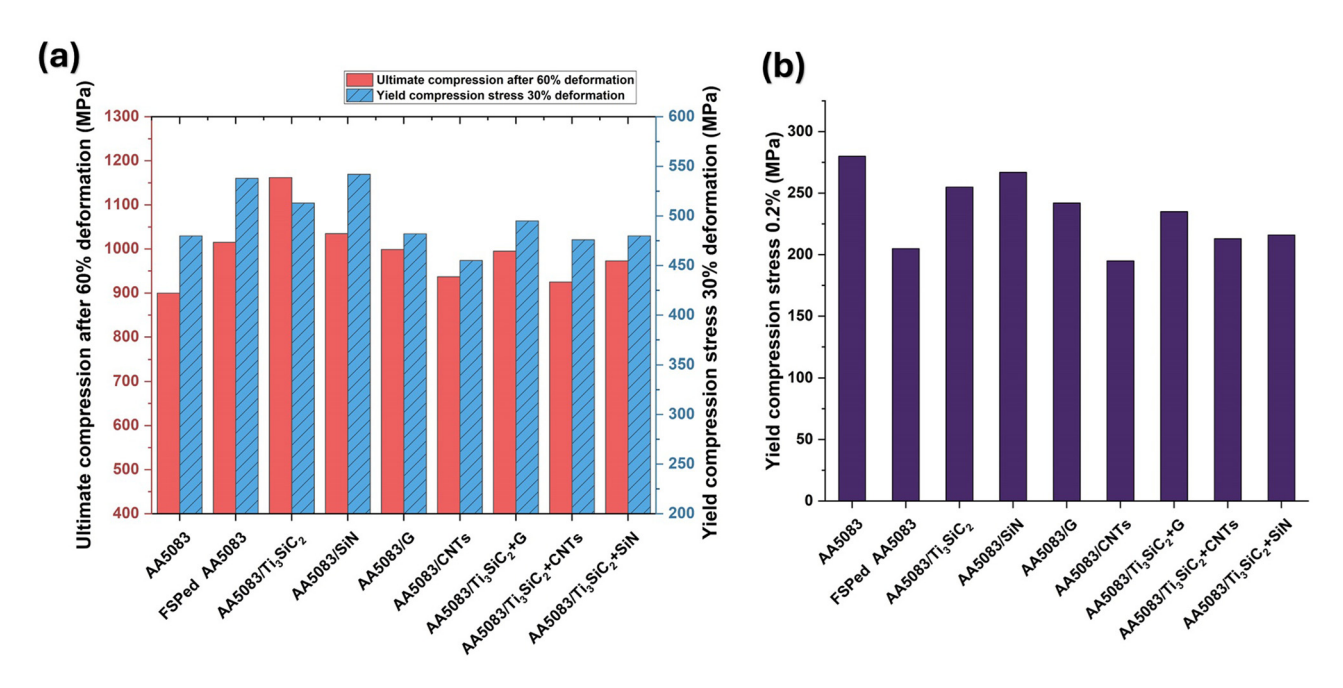


**Figure 10:** UCS at different deformations: (a) UCS at 30 and 60% deformation and (b) yield strength at  $\sigma_{0.2\%}$ .

multiple reinforcements with varying sizes and morphologies can be challenging, potentially leading to localized stress concentrations. Finally, introducing multiple reinforcements can increase the likelihood of microstructural defects like voids or microcracks, which act as stress concentrators and reduce the composite's ultimate strength.

# 3.4 Dynamic properties

The results obtained from the free vibration test focused on the damping ratio and dynamic modulus and their impact on the overall dynamic behavior of the investigated samples. Figure 11 illustrates the first mode's natural frequency and deflection shape; hence, the investigation used the Euler–Bernoulli beam theory to calculate the dynamic

properties of the studied composites. These properties offer valuable insights into the materials' behavior under dynamic loading conditions. The damping ratio ( $\zeta$ %) reflects the energy dissipation during vibration, with higher values indicating faster vibration decay. The dynamic Young's modulus of the composite samples is determined by utilizing the first mode natural frequency derived from a free vibration test and the logarithmic decrement ( $\delta$ ) and damping ratio ( $\zeta$ ). The experimental results of the free vibration test are plotted and analyzed as shown in Figures 12 and 13; thus, they represent the time domain in the transient response of the investigated, including a base AA5083 aluminum alloy and composites reinforced with different particles, as a free vibration test determined.

The logarithmic decrement ( $\delta$ ) characterizes the decay rate of free vibrations. It is calculated using the following equation:

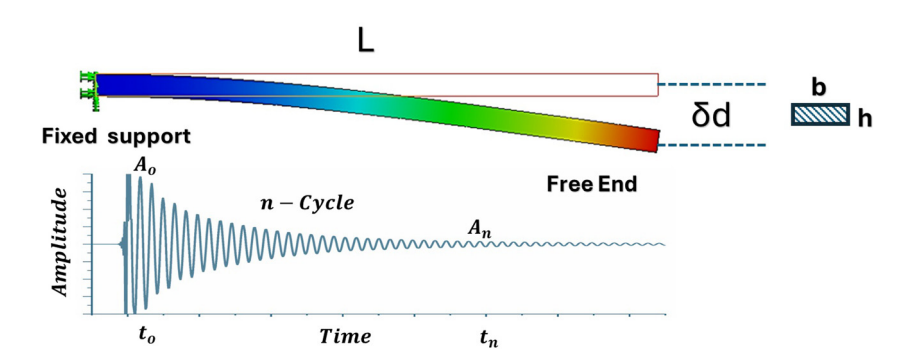


Figure 11: First mode natural frequency of the cantilever beam in the free vibration.

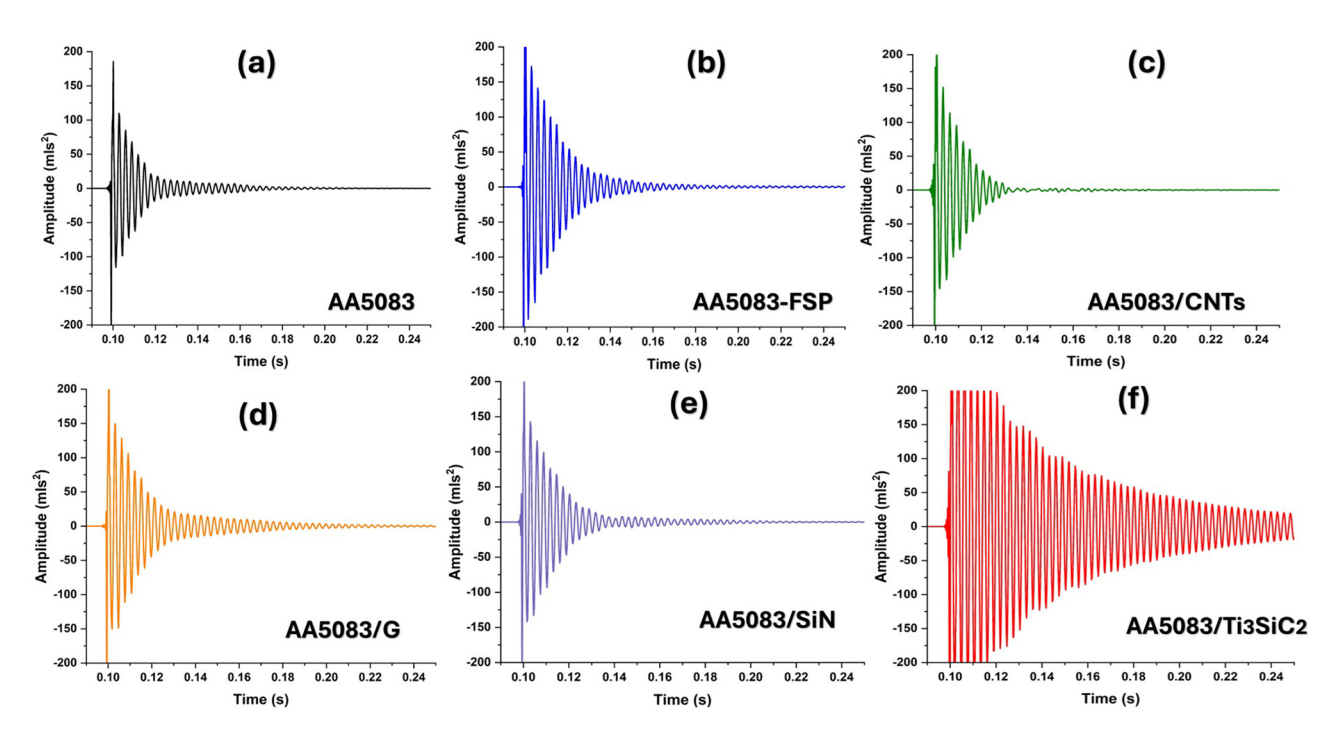


Figure 12: Time-domain decay response: (a) base alloy AA5083, (b) FSPed, (c) single composite AA5083/CNTs, (d) single composite AA5083/graphene, (e) single composite AA5083/SiN, and (f) single composite AA5083/max-phase Ti<sub>3</sub>SiC<sub>2</sub>.

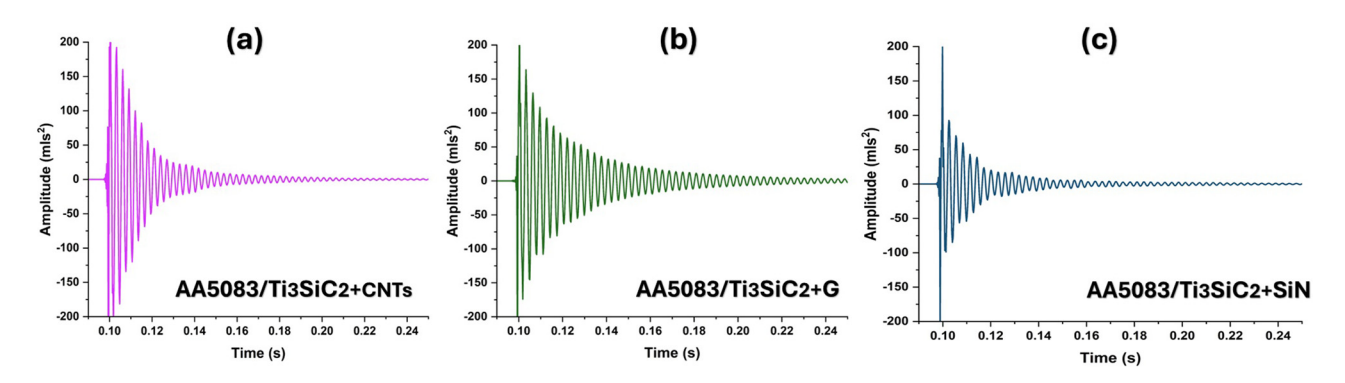


Figure 13: Time-domain decay response of the hybrid composites: (a) composite AA5083/Ti<sub>3</sub>SiC<sub>2</sub>+CNTs, (b) composite AA5083/Ti<sub>3</sub>SiC<sub>2</sub>+graphene, and (c) AA5083/Ti<sub>3</sub>SiC<sub>2</sub>+SiN.

$$\delta = \frac{1}{n} \ln \frac{A_0}{A_n},\tag{1}$$

where  $\delta$  is the logarithmic decrement (unitless),  $A_{\rm o}$  is the initial amplitude of the vibration,  $A_n$  is the amplitude of the vibration after a certain number of cycles (typically chosen at a specific time interval), and *n* is the number of cycles

The damping ratio ( $\zeta$ ) represents the energy dissipated in each vibration cycle. It is related to the logarithmic decrement by

$$\zeta = \frac{\delta}{\sqrt{4\pi^2 + \delta^2}},\tag{2}$$

where  $\zeta$  is the damping ratio (unitless).

Calculating dynamic Young's modulus (E) using Euler-Bernoulli beam theory assumes small deflections.

$$E = \frac{4\pi^2 \times f_{\rm n}^2 \times \rho \times L^4}{b \times h^3 \times (1 + (6 \times \zeta^2))},$$
 (3)

where E is the dynamic Young's modulus (Pa),  $f_n$  is the first mode natural frequency (Hz),  $\rho$  is the density of fabricated composite (kg/m $^3$ ), L, b, and h are the beam's length, width, and thickness (m), and  $\zeta$  is the damping ratio.

Loss factor  $(\eta)$  relates to the energy dissipation per cycle and is associated with the damping ratio by

$$\eta = 2\zeta,\tag{4}$$

where  $\eta$  is the loss factor (unitless) and loss modulus (E''). This represents the imaginary component of the complex modulus and reflects the energy dissipation. It is calculated using the following equation:

$$E'' = E'\eta, \tag{5}$$

where *E*" is the loss modulus (Pa) and storage modulus (*E*'). This represents the real component of the complex modulus and reflects the elastic energy storage. It is related to the dynamic Young's modulus by

$$E' = \frac{E}{1 + \eta^2},\tag{6}$$

where E' is the storage modulus (Pa).

The damping ratio and loss modulus usually correlate positively. High-damping ratio materials have a larger loss modulus, suggesting greater energy dissipation. FSP shows a slight increase in both damping ratio (2.93%) and natural frequency (2.0%) compared to the base alloy, indicating a minor improvement in energy dissipation and stiffness. In the case of single composites, the CNT reinforcement offers the most significant improvement in both damping ratio (4.72%) and natural frequency (4.8%), suggesting excellent energy absorption and enhanced stiffness. SiN reinforcement also demonstrates a substantial increase in natural frequency (4.4%) and a moderate rise in damping ratio (4.04%), as shown in Figure 14. The high damping ratios in single composites of SiN and CNTs can be attributed to two primary processes. First, both materials employ

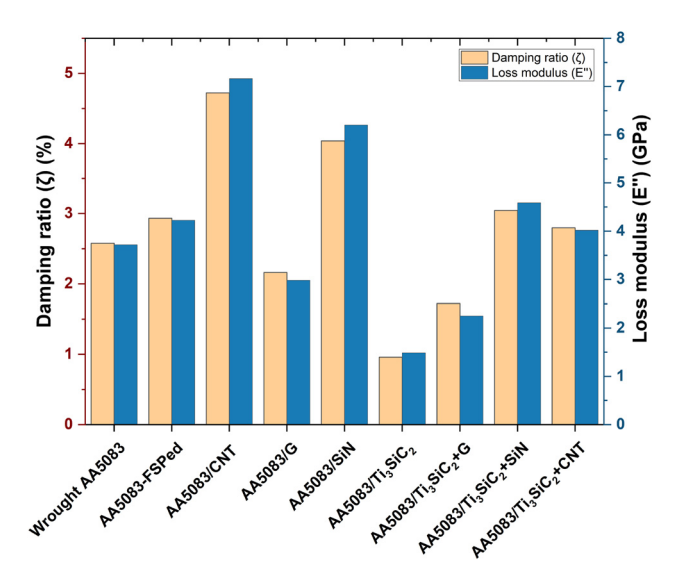


**Figure 14:** Damping ratio ( $\zeta$ ) and dynamic modulus (E'') of pure AA5083, FSPed AA5083, single composites with CNTs, graphene, SiN, and hybrid composites with max-phase Ti<sub>3</sub>SiC<sub>2</sub> particles combined with CNTs, graphene, and SiN.

internal friction processes to disperse vibrational energy. The complicated internal structure of SiN allows for friction between its boundaries, but the high aspect ratio and flexibility of CNTs enable them to slide, bend, and suffer internal friction within the matrix [45,46]. Furthermore, the robust interface between these reinforcements and the aluminum matrix forms a constriction point for transmitting vibration energy. The microscopic motions and separation at this boundary also contribute to energy dissipation, increasing the total damping ratio [47]. Although the exact mechanisms may include an intricate interaction of these parameters, it is evident that both SiN and CNTs have unique benefits as reinforcements for achieving high damping qualities in these composites.

Graphene reinforcement exhibits the least impact, showing a negligible change in natural frequency and a slight decrease in damping ratio. On the other hand, the combination of Ti<sub>3</sub>SiC<sub>2</sub> max-phases with CNTs (Ti<sub>3</sub>SiC<sub>2</sub>/CNT) exhibits the highest natural frequency (353.08 Hz), a significant improvement (5.8%) compared to the base alloy. This indicates the most remarkable enhancement in stiffness. However, it has the lowest damping ratio (0.96%), suggesting reduced energy dissipation capabilities.

Figure 15 shows the first mode natural frequency of various materials derived from aluminum alloy AA5083. Generally, stiffer materials exhibit higher natural frequencies. Composites reinforced with CNTs, SiN, and max-phase Ti<sub>3</sub>SiC<sub>2</sub>+CNTs possess a higher natural frequency compared to the unreinforced aluminum alloy (AA5083) due to their increased stiffness. This enhancement likely originates from the inherent stiffness of CNTs and SiN, which act as reinforcements within the aluminum matrix. In the case of

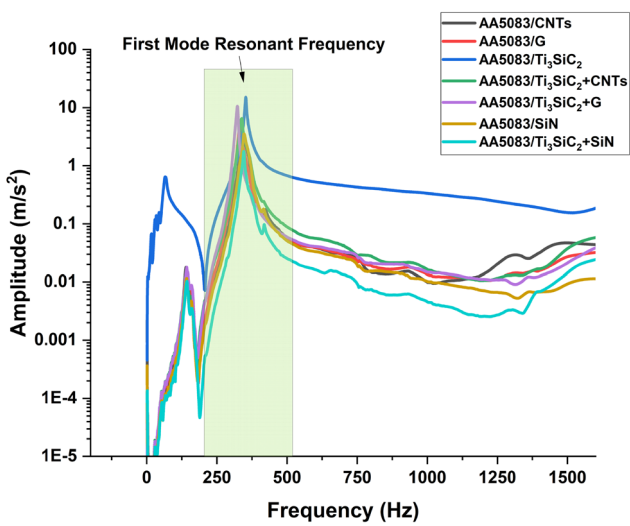
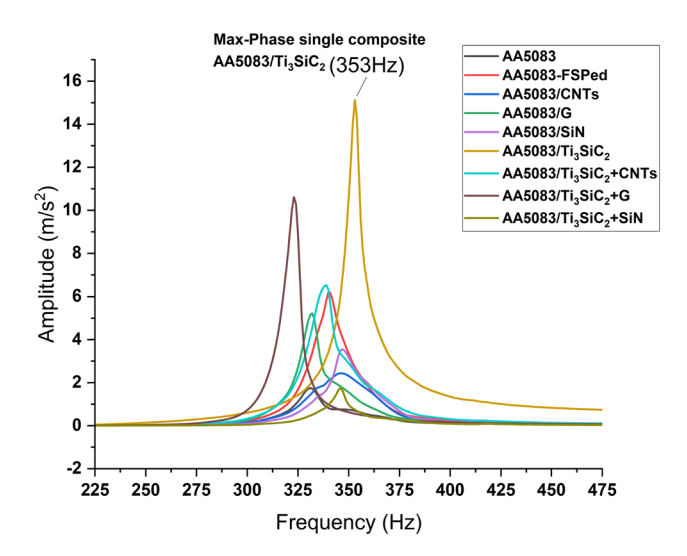


Figure 15: FRF of the single and hybrid composite matrix.



**Figure 16:** Frequency domain plot of the investigated samples in the frequency range 300–400 Hz.

Ti<sub>3</sub>SiC<sub>2</sub>/CNTs, the combination of Ti<sub>3</sub>SiC<sub>2</sub> stiffness and the high strength and aspect ratio of CNTs likely leads to a particularly stiff composite material.

Conversely, the lower natural frequency observed in the single composite AA5083/Ti<sub>3</sub>SiC<sub>2</sub> compared to the unreinforced alloy could be attributed to the presence of voids or defects within the composite, acting as stress concentrators and reducing stiffness. A weak interfacial bond between the Ti<sub>3</sub>SiC<sub>2</sub> reinforcement and the aluminum matrix could contribute to this composite's lower stiffness. Figure 16 shows the value of first mode resonant frequencies in the frequency domain plot of the investigated samples; thus, the addition of Ti<sub>3</sub>SiC<sub>2</sub> to SiN or graphene (Ti<sub>3</sub>SiC<sub>2</sub>/SiN and Ti<sub>3</sub>SiC<sub>2</sub>/G) offers a balanced approach. These composites show increased natural frequencies (1.5-3.0%) compared to the base alloy while maintaining moderate damping ratios. The pure AA5083 alloy has a baseline dynamic modulus of 72.09 GPa. The FSP shows minimal impact (72.00 GPa for 5083-FSPed), suggesting this technique does not significantly alter the dynamic modulus. Compared to the base alloy (AA5083), 5083-FSPed and single composites reinforced with SiN and CNTs exhibit a slight improvement in both natural frequency and dynamic modulus, suggesting increased stiffness by up to 5.2% (SiN) for these composites; hence these results are consistent with the studies of Liu et al. [48]. This can likely be attributed to the reinforcement mechanisms, where friction stir processing refines the grain structure of the aluminum matrix (5083-FSPed), and SiN and CNTs, due to their inherent stiffness, improve the composite's overall stiffness.

On the other hand, the single composite AA5083/graphene and hybrid AA5083/ $Ti_3SiC_2+G$  demonstrate relatively lower stiffness and dynamic properties than other

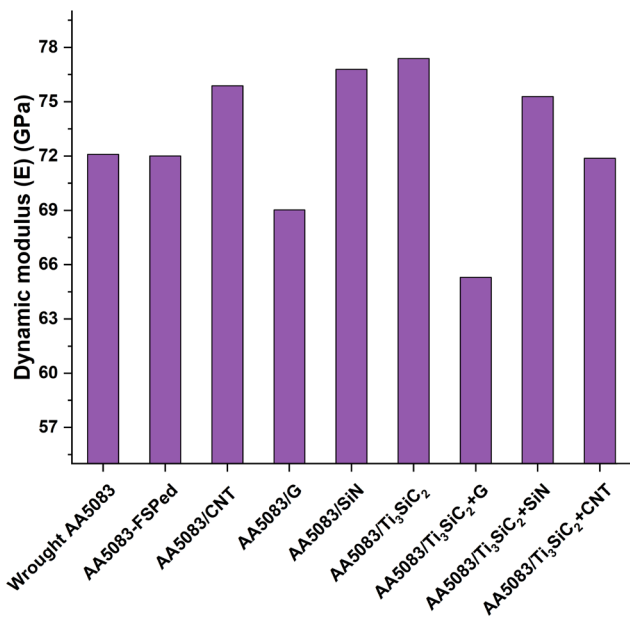


Figure 17: Dynamic modulus of the investigated metal matrix.

reinforced composites. This can be due to the weak interfacial bonding between the graphene platelets and the aluminum matrix. A weak interface between the matrix and the graphene restricts the efficient transfer of stress, affecting the enhancement of reinforcement and overall improvement in stiffness. Graphene layers may undergo restacking or agglomeration during processing, which can diminish their effectiveness as reinforcements (Figure 17). Interestingly, the single composite reinforced with maxphase Ti<sub>3</sub>SiC<sub>2</sub> shows a higher natural frequency but a lower dynamic modulus than the base alloy. This could be due to the contrasting properties of Ti<sub>3</sub>SiC<sub>2</sub>. While it might enhance rigidity, its potentially brittle nature could introduce microcracks, reducing the material's overall stiffness. However, the hybrid composites incorporating Ti<sub>3</sub>SiC<sub>2</sub> with Ti<sub>3</sub>SiC<sub>2</sub>/G, Ti<sub>3</sub>SiC<sub>2</sub>/ SiN, and Ti<sub>3</sub>SiC<sub>2</sub>/CNT seem promising. These composites generally demonstrate a well-balanced combination of damping (indicated by  $\zeta$ ) and stiffness (E). Notably, Ti<sub>3</sub>SiC<sub>2</sub>/CNT potentially offers the highest improvement in stiffness (13.5%) by combining the high stiffness of CNTs with Ti<sub>3</sub>SiC<sub>2</sub>, creating a potentially stiffer composite material. The behavior of the Ti<sub>3</sub>SiC<sub>2</sub> composite emphasizes the need to consider factors beyond just the reinforcement material's stiffness, as interface bonding and microcrack formation can significantly influence the overall response. Hybrid composites incorporating Ti<sub>3</sub>SiC<sub>2</sub> with various materials appear promising for balancing stiffness and damping.

Table 1 illustrates the improvement in the studied composites' microstructure, mechanical, and dynamic properties related to the base matrix AA5083. The presented data

14 — Sahw S. Almutairi et al. DE GRUYTER

Table 1: Effect of reinforcement on the improvement in the different properties

	Improvement % with respect to base alloy AA5083					
Samples	Damping ratio (ζ)	Natural frequency (f <sub>n</sub> )	Dynamic modulus ( <i>E</i> )	YCS σ <sub>0.2</sub>	UCS 60%	AVG grain size (reduction)
FSPed AA5083	13.73	1.99	-0.12	17.85	12.77	-97.90
AA5083 CNTs	83.07	4.82	5.25	12.5	4.11	-98.03
AA5083/graphene	-16.15	-0.02	-4.25	14.64	11	-98.11
AA5083/SiN	56.6	4.33	6.52	15.35	15	-98.27
AA5083/Ti <sub>3</sub> SiC <sub>2</sub>	-62.76	5.82	7.34	25.35	29.11	-98.23
AA5083/Ti <sub>3</sub> SiC <sub>2</sub> +G	-33.16	-3.15	-9.42	25	10.55	-98.53
AA5083/Ti <sub>3</sub> SiC <sub>2</sub> +SiN	18.09	3.46	4.42	12.85	8.11	-98.56
AA5083/Ti <sub>3</sub> SiC <sub>2</sub> +CNT	8.46	1.54	-0.29	15.71	2.77	-98.1

elucidate the impact of the FSP and various reinforcements on the ultimate compression strength of AA5083 aluminum alloy after 60 and 30% deformation. FSP significantly enhances the alloy's performance, showing a 12.77 and 12.55% improvement in ultimate compression strength at 60 and 30% deformation, respectively, due to grain refinement and microstructural homogenization. Among the single composites, the addition of max-phase Ti<sub>3</sub>SiC<sub>2</sub> particles demonstrates the most substantial improvement, with a 29.11% increase at 60% deformation and a 7.53% increase at 30% deformation, attributed to strong interfacial bonding and effective hindrance of dislocation motion. SiN also significantly improves both 60% (15%) and 30% (13.59%) deformation strengths. While graphene reinforcement shows a notable 11% improvement at 60% deformation, CNTs exhibit a mixed effect with a 4.11% improvement at 60% deformation but a 4.6% reduction at 30% deformation. Hybrid composites combining Ti<sub>3</sub>SiC<sub>2</sub> with either graphene, SiN, or CNTs, generally show improvements at 60% deformation but less pronounced or even negative effects at 30% deformation, suggesting that the hybrid effect is not always additive and can be deformation dependent. Overall, these findings highlight the potential of FSP and reinforcement additions, particularly Ti<sub>3</sub>SiC<sub>2</sub> and SiN, to enhance the ultimate compression strength of AA5083.

#### 4 Conclusion

 This study investigated the effects of incorporating maxphase Ti<sub>3</sub>SiC<sub>2</sub> particles and various nanoparticle reinforcements (graphene, CNTs, and SiN) on the mechanical and dynamic properties of AA5083 aluminum alloy. The FSP was employed to fabricate the MMCs, resulting in significant grain refinement and microstructural homogenization. This led to substantial improvements in the mechanical

- properties, notably a 22% increase in yield compression stress and a 13% increase in ultimate compression strength compared to the base AA5083 alloy.
- The addition of reinforcements further enhanced the composites' performance. Among the single composites, AA5083/max-phase Ti<sub>3</sub>SiC<sub>2</sub> exhibited the most significant improvement, with a 25% increase in yield strength and a 30% increase in ultimate compression strength compared to the FSPed AA5083. This enhancement is attributed to the strong interfacial bonding between the Ti<sub>3</sub>SiC<sub>2</sub> particles and the aluminum matrix, effectively hindering dislocation motion.
- While hybrid composites showed promising yield strength, their ultimate compression strength was generally lower than their single-reinforcement counterparts, suggesting a potential trade-off between strength and ductility.
- The addition of reinforcement particles generally increased both natural frequency ( $f_n$ ) and dynamic modulus (E), indicating enhanced stiffness and vibration resistance. However, this improvement came at the expense of a reduced damping ratio ( $\zeta$ ), signifying lower energy dissipation capacity. The AA5083/max-phase Ti<sub>3</sub>SiC<sub>2</sub> composite exemplified this trend, exhibiting the highest  $f_n$  (351.08 Hz) and E (77.39 GPa) among all the samples but also the lowest damping ratio (0.96%).

**Acknowledgments:** This project was funded by the Deanship of Scientific Research (DSR) at King Abdulaziz University, Jeddah, under grant No. (GPIP:134-135-2024). The authors, therefore, gratefully acknowledge with thanks DSR technical and financial support.

**Funding information:** This project was funded by the Deanship of Scientific Research (DSR) at King Abdulaziz University, Jeddah, under grant no. GPIP:134-135-2024. The authors, gratefully acknowledge the DSR technical and financial support.

Author contributions: All authors have accepted responsibility for the entire content of this manuscript and approved its submission.

**Conflict of interest:** The authors state no conflict of interest.

Data availability statement: The datasets generated and/ or analyzed during the current study are available from the corresponding author on reasonable request.

# References

- Sunnapu CS, Kolli M. Experimental investigation of Al 5083 alloy using friction stir welding process through taguchi method. Int J Interact Des Manuf. 2024.
- Jebaraj AV, Aditya KVV, Kumar TS, Ajaykumar L, Deepak CR. Mechanical and corrosion behaviour of aluminum alloy 5083 and its weldment for marine applications. Mater Today: Proc. 2020;22:1470-8.
- Du R, Mareau C, Ayed Y, Giraud E, Dal Santo P. Experimental and numerical investigation of the mechanical behavior of the AA5383 alloy at high temperatures. J Mater Process Technol. 2020;281:116609.
- [4] Booth GH, Cooper AW, Tiller AK. Corrosion of mild steel in the tidal waters of the thames estuary. II. Results of two years' immersion. J Appl Chem. 1965;15(6):250-6.
- Wahid MA, Siddiquee AN, Khan ZA. Aluminum alloys in marine construction: characteristics, application, and problems from a fabrication viewpoint. Mar Syst Ocean Technol. 2020;15(1):70-80.
- Vorontsov AV. Corrosion resistance of aluminum-magnesium alloy AA5083 welded joint after high-speed laser welding. AIP Conf Proc. 2020:2310(1):020350.
- Behnagh RA, Besharati Givi MK, Akbari M. Mechanical properties, corrosion resistance, and microstructural changes during friction stir processing of 5083 aluminum rolled plates. Mater Manuf Process. 2012:27(6):636-40.
- Hashmi AW, Mehdi H, Mishra RS, Mohapatra P, Kant N, Kumar R. Mechanical properties and microstructure evolution of AA6082/SiC nanocomposite processed by multi-pass FSP. Trans Indian Inst Met. 2022;75(8):2077-90.
- Rasouli S, Behnagh RA, Dadvand A, Saleki-Haselghoubi N. Improvement in corrosion resistance of 5083 aluminum alloy via friction stir processing. Proc Inst Mech Eng Part L: J Mater Des Appl. 2014;230(1):142-50.
- [10] Nieto A, Yang H, Jiang L, Schoenung JM. Reinforcement size effects on the abrasive wear of boron carbide reinforced aluminum composites. Wear. 2017;390-391:228-35.
- [11] Reddy MP, Himyan MA, Ubaid F, Shakoor RA, Vyasaraj M, Gururaj P, et al. Enhancing thermal and mechanical response of aluminum using nanolength scale TiC ceramic reinforcement. Ceram Int. 2018;44(8):9247-54.
- [12] Ahmed MMZ, Ataya S, El-Sayed Seleman MM, Ammar HR, Ahmed E. Friction stir welding of similar and dissimilar AA7075 and AA5083. J Mater Process Technol. 2017;242:77-91.
- [13] Moustafa EB, Melaibari A, Alsoruii G, Khalil AM, Mosleh AO. Tribological and mechanical characteristics of AA5083 alloy

- reinforced by hybridising heavy ceramic particles Ta<sub>2</sub>C & VC with light GNP and Al<sub>2</sub>O<sub>3</sub> nanoparticles. Ceram Int. 2022;48(4):4710-21.
- Nagaraja S, Nagegowda KU, Kumar VA, Alamri S, Afzal A, Thakur D, et al. Influence of the fly ash material inoculants on the tensile and impact characteristics of the aluminum AA 5083/7.5SiC composites. Materials. 2021;14(9):2452.
- Peel M, Steuwer A, Preuss M, Withers PJ. Microstructure, mechanical [15] properties and residual stresses as a function of welding speed in aluminium AA5083 friction stir welds. Acta Mater. 2003;51(16):4791-801.
- Kunze JM, Bampton CC. Challenges to developing and producing MMCs for space applications. JOM. 2001;53(4):22-5.
- Abushanab WS, Moustafa EB, Goda ES, Ghandourah E, Taha MA, Mosleh AO. Influence of vanadium and niobium carbide particles on the mechanical, microstructural, and physical properties of AA6061 aluminum-based mono- and hybrid composite using FSP. Coatings. 2023;13(1):142.
- [18] Abdelhady SS, Elbadawi RE, Zoalfakar SH. Investigation of the microstructure, mechanical and wear performance of friction stirprocessed AA6061-T6 plate reinforced with B<sub>4</sub>C particles surface composite. J Compos Mater. 2023;57(14):2297-310.
- Ramesh B, Elsheikh AH, Satishkumar S, Shaik AM, Djuansjah J, Ahmadein M, et al. The influence of boron carbide on the mechanical properties and bonding strength of B<sub>4</sub>C/nickel 63 coatings of brake disc. Coatings. 2022;12(5):663.
- [20] Selvamani ST, Bakkiyaraj M, Palani S, Yoganandan G. Corrosion behavior and analysis on friction stir welded aluminium matrix composites. Surf Topogr: Metrol Prop. 2022;10(2):025036.
- [21] Moustafa EB, Melaibari A, Basha M. Wear and microhardness behaviors of AA7075/SiC-BN hybrid nanocomposite surfaces fabricated by friction stir processing. Ceram Int. 2020;46(10, Part B):16938-43.
- Hosseini SA, Ranjbar K, Dehmolaei R, Amirani AR. Fabrication of Al5083 surface composites reinforced by CNTs and cerium oxide nano particles via friction stir processing. J Alloy Compd. 2015;622:725-33.
- [23] Li M, Ma K, Jiang L, Yang H, Lavernia EJ, Zhang L, et al. Synthesis and mechanical behavior of nanostructured Al 5083/n-TiB2 metal matrix composites. Mater Sci Eng: A. 2016;656:241-8.
- [24] Stein J, Lenczowski B, Fréty N, Anglaret E. Mechanical reinforcement of a high-performance aluminium alloy AA5083 with homogeneously dispersed multi-walled carbon nanotubes. Carbon. 2012;50(6):2264-72.
- [25] Zayed EM, El-Tayeb NSM, Ahmed MMZ, Rashad RM. Development and characterization of AA5083 reinforced with SiC and Al<sub>2</sub>O<sub>3</sub> particles by friction stir processing. In: Öchsner A, Altenbach H, editors. Engineering design applications. Cham: Springer International Publishing; 2019. p. 11-26.
- [26] Heidarpour A. Fabrication and characterization of A5083-WC- Al<sub>2</sub>O<sub>3</sub> surface composite by friction stir processing. J Mater Eng Perform. 2019;28(5):2747-53.
- Ahmed HM, Ahmed HAM, Hefni M, Moustafa EB. Effect of grain refinement on the dynamic, mechanical properties, and corrosion behaviour of Al-Mg alloy. Metals. 2021;11(11):1825.
- Moustafa EB. Dynamic characteristics study for surface composite of AMMNCs matrix fabricated by friction stir process. Materials. 2018;11(7):1240.
- **[29]** Srikanth N, Kurniawan LA, Gupta M. Effect of interconnected reinforcement and its content on the damping capacity of aluminium matrix studied by a new circle-fit approach. Compos Sci Technol. 2003;63(6):839-49.

- [30] Shivakumar SP, Sharan AS, Sadashivappa K. Experimental investigations on vibration properties of aluminium matrix composites reinforced with iron oxide particles. Appl Mech Mater. 2019;895:122–6.
- [31] Rozhbiany FAR, Jalal SR. The effectiveness of reinforcement and processing on mechanical properties, wear behavior and damping response of aluminum matrix composites. J High Temp Mater Process. 2019;38(2019):927–39.
- [32] Venkatesan S, Xavior MA. Characterization on aluminum alloy 7050 metal matrix composite reinforced with graphene nanoparticles. Proc Manuf. 2019;30:120–7.
- [33] Seyed Pourmand N, Asgharzadeh H. Aluminum matrix composites reinforced with graphene: a review on production, microstructure, and properties. Crit Rev Solid State Mater Sci. 2020;45(4):289–337.
- [34] Singla D, Amulya K, Murtaza Q. CNT reinforced aluminium matrix composite a review. Mater Today: Proc. 2015;2(4):2886–95.
- [35] Li NY, Yang C, Li CJ, Guan HD, Fang D, Tao JM, et al. Carbon nanotubes reinforced aluminum matrix composites with high elongation prepared by flake powder metallurgy. Diam Relat Mater. 2020;107:107907.
- [36] Mazahery A, Shabani MO. Nano-sized silicon carbide reinforced commercial casting aluminum alloy matrix: experimental and novel modeling evaluation. Powder Technol. 2012;217:558–65.
- [37] Moustafa EB, Abushanab WS, Melaibari A, Mikhaylovskaya AV, Abdel-Wahab MS, Mosleh AO. Nano-surface composite coating reinforced by Ta<sub>2</sub>C, Al<sub>2</sub>O<sub>3</sub> and MWCNTs nanoparticles for aluminum base via FSP. Coatings. 2021;11(12):1496.
- [38] Moustafa EB. Vibration-damped aluminum article and method of forming the article. King Abdulaziz University, US Pat., 11413701B1, 2022.
- [39] Moustafa EB, Almitani KH. Detecting damage in carbon fibre composites using numerical analysis and vibration measurements. Lat Am J Solids Struct. 2021;18(3):1–17.

- [40] Abushanab WS, Moustafa EB, Youness RA. Evaluation of the dynamic behavior, elastic properties, and in vitro bioactivity of some borophosphosilicate glasses for orthopedic applications. J Non-Cryst Solids. 2022;586:121539.
- [41] Mousa G, Basha M, Moustafa EB. Evaluation of the mechanical and dynamic properties of scrimber wood produced from date palm fronds. J Mech Behav Mater. 2024;33(1):20220305.
- [42] Mehdi H, Mishra RS. Modification of microstructure and mechanical properties of AA6082/ZrB<sub>2</sub> processed by multipass friction stir processing. J Mater Eng Perform. 2023;32(1):285–95.
- [43] Mehdi H, Mishra RS. Consequence of reinforced SiC particles on microstructural and mechanical properties of AA6061 surface composites by multi-pass FSP. J Adhes Sci Technol. 2022;36(12):1279–98.
- [44] Muñoz-Morris MA, Calderón N, Gutierrez-Urrutia I, Morris DG. Matrix grain refinement in Al–TiAl composites by severe plastic deformation: influence of particle size and processing route. Mater Sci Eng: A. 2006;425(1):131–7.
- [45] Lass EA, Koratkar NA, Ajayan PM, Wei BQ, Keblinski P. Damping and stiffness enhancement in composite systems with carbon nanotubes films. Proc. 2022;740:I11.
- [46] Zhou X, Shin E, Wang KW, Bakis CE. Damping characteristics of carbon nanotube based composites. Chicago, Illinois, USA: ASMEDC; 2003. p. 1925–35.
- [47] Liew KM, Kai MF, Zhang LW. Mechanical and damping properties of CNT-reinforced cementitious composites. Compos Struct. 2017;160:81–8.
- [48] Liu ZY, Xiao BL, Wang WG, Ma ZY. Developing high-performance aluminum matrix composites with directionally aligned carbon nanotubes by combining friction stir processing and subsequent rolling. Carbon. 2013;62:35–42.